

**Multi-Stimuli-Responsive Self-Healing Metallo-Supramolecular Polymer Nanocomposites**

Journal:	<i>Journal of Materials Chemistry A</i>
Manuscript ID	TA-ART-12-2015-010694.R1
Article Type:	Paper
Date Submitted by the Author:	22-Jan-2016
Complete List of Authors:	Zheng, Qifeng; University of Wisconsin-Madison, Materials Science and Engineering Ma, Zhenqiang; University of Wisconsin at Madison, Electrical and Computer Engineering Gong, Shaoqin; University of Wisconsin-Madison, Department of Biomedical

Multi-Stimuli-Responsive Self-Healing Metallo-Supramolecular Polymer Nanocomposites

Qifeng Zheng,^{a,b} Zhenqiang Ma,^c and Shaoqin Gong^{*,a,b,d}

^a *Department of Material Science and Engineering, University of Wisconsin–Madison, WI
53706, USA.*

^b *Wisconsin Institute for Discovery, University of Wisconsin–Madison, WI 53715, USA*

^c *Department of Electrical Engineering, University of Wisconsin–Madison, WI 53706, USA*

^d *Department of Biomedical Engineering, University of Wisconsin–Madison, WI 53706, USA*

*Corresponding author: Shaoqin Gong. Email: sgong@engr.wisc.edu; Tel: +01 6083164311.

Abstract

The self-healing capability is particularly desirable for multifunctional polymeric materials because it can make the materials more reliable, reduce repair costs, and extend the lifetime in many applications. Herein, a multi-stimuli responsive self-healing metallo-supramolecular polymer nanocomposite exhibiting superior mechanical properties was developed and demonstrated. Terpyridine ligand-terminated polyurethane (PU) was prepared by *in situ* polymerization on the surface of multi-walled carbon nanotubes (CNTs). The terpyridine ligand-terminated CNT/PU prepolymers were dynamically crosslinked with the metal ion Zn^{2+} to obtain metallo-supramolecular polymer nanocomposite. The tensile strength and tensile strain-at-break of the CNT/PU polymer nanocomposite increased from 14.2 MPa and 620% to 22.8 MPa and 1076%, respectively, with the addition of Zn^{2+} . The Zn^{2+} -coordinated metallo-supramolecular polymer nanocomposite showed a rare combination of strong, tough, and elastic mechanical properties and was able to self-heal via multiple stimuli, including remotely controlled near infrared (NIR) light (4.2 mW/mm², 30 min), relatively low temperatures (90°C, 1 hr), and/or solvents, all with excellent healing efficiencies (i.e., higher than 93%) and short healing times. Therefore, this unique multi-stimuli responsive self-healing metallo-supramolecular polymer nanocomposite has the potential to provide advances in structural component, microelectronic and sporting equipment applications, to name just a few.

Keywords: self-healing, metallo-supramolecular, carbon nanotubes, near infrared light, superior mechanical properties

1. Introduction

Polymeric materials have been used in a broad range of applications,^{1, 2} such as medical devices, transportation vehicles, microelectronics, clothing, sporting equipment, artificial skins, etc., due to their low density, excellent machinability, high flexibility, and biocompatibility. However, in comparison with metallic or other types of inorganic materials, polymeric materials may be more prone to structural damage, including crack formation, because of their relatively low strength and higher environmental susceptibility, which might lead to the failure of the materials. Therefore, there is a high demand for self-healing polymeric materials that can repair themselves after structural damage, which can significantly reduce the cost of repairs and extend the service life of expensive components/devices.

Over the last decade, great efforts have been made to develop self-healing polymeric materials.^{3, 4} One of the earlier self-healing approaches employed encapsulated reactive ingredients that were embedded in a polymer matrix.⁵⁻⁷ Formation of cracks/scratches would trigger a release of the reactive ingredients, which would typically polymerize by themselves or react with the polymer matrix, thereby enabling self-healing of the damaged materials. This type of self-healing material can heal itself autonomously and in a timely fashion; however, such repairs cannot be repeated because the healing agents are depleted locally after the first repair. This approach was later improved by utilizing microvascular networks containing healing agents, which could be delivered to the crack area, thereby making repeated healing possible.^{8, 9} In recent years, intrinsic self-healing materials based on dynamic covalent bonds (e.g., Diels–Alder reaction,^{10, 11} [2+2] cycloaddition,¹² or disulfide moiety¹³) and non-covalent interactions (e.g., hydrogen bonding,^{14, 15} host–guest interaction,¹⁶ π – π stacking,¹⁷ or ionic interaction¹⁸) have attracted great attention owing to their reversible nature, which allows for repetitive repairs. Self-healing systems based on non-covalent interactions are of particular

interest because they usually exhibit high healing efficiencies and multi-stimuli responsive characteristics.

In principle, metal–ligand interactions, which can dynamically associate or dissociate due to their moderate bond energy, can also be used to build self-healing systems. In fact, self-healing systems based on metal–ligand interactions have been discovered in nature. For instance, the self-healing capability exhibited by mussel byssus threads is attributed to the reversible iron dihydroxy-phenylalanine interaction.^{19, 20} Moreover, Weng et al. reported healable metallo-supramolecular gels based on interactions between the 2,6-bis (1,2,3-triazol-4-yl) pyridine ligands incorporated into the polymer backbone and metal ions (Zn^{2+} and/or Eu^{3+}).²¹ Yu et al. developed a pH-responsive self-healing graphene oxide/polymer hydrogel crosslinked via metal–ligand interactions.²² Up to now, metal–ligand complexes have seldom been used in developing self-healing polymer films/coatings owing to the fact that a compromise between mechanical properties and self-healing capabilities must be made.²³ In 2011, Rowan and coworkers reported the first linear metallo-supramolecular elastomer that was capable of healing a crack when exposed to ultraviolet (UV) light and/or heated up to 220 °C.²⁴ Recently, Schubert and coworkers reported a thermally self-healing polymer bearing ligands in the side chains that can form crosslinks with Fe^{2+} ions.²³ However, the mechanical strengths of these self-healing metallopolymers were generally compromised, which may limit their applications. Therefore, developing novel self-healing metallo-supramolecular materials with superior mechanical properties and excellent healing efficiencies still remains a critical challenge.

Carbon nanotubes (CNTs) have been widely used as reinforcing fillers for polymers due to their outstanding mechanical properties.^{25, 26} Furthermore, CNTs exhibit superior electrical and thermal conductivity, and excellent near infrared (NIR) light absorption and thermal conversion capabilities due to their large π -conjugated sp^2 carbon network.²⁷⁻²⁹

Inspired by the unique properties possessed by CNTs, we developed a novel Zn^{2+} -coordinated metallo-supramolecular CNT/polyurethane (PU) self-healing nanocomposite that showed a rare combination of strong, tough, and elastic mechanical properties and was able to self-heal via multiple stimuli, including remotely controlled NIR light, relatively low temperatures, and/or solvents, all with excellent healing efficiencies and short healing times. To the best of our knowledge, this is the first time self-healing of a metallo-supramolecular polymer film triggered by remotely controlled and localized NIR light has been reported. To prepare the self-healing metallo-supramolecular CNT/PU nanocomposite, terpyridine ligand-terminated PU was first synthesized via *in situ* polymerization on the surface of CNTs (Scheme 1); the resulting terpyridine ligand-terminated PU was subsequently crosslinked with the metal ion Zn^{2+} (Scheme 2).

2. Experimental Section

Materials

Hydroxyl-functionalized multi-walled CNTs (OH content: 3.70 wt%; outer diameter: 8–15nm; length: 10–50 μm) were obtained from Cheap Tubes (Brattleboro, VT). 6-Amino-1-hexanol (97 wt%), 1,6-hexyldiisocyanate (HDI), 6-amino-1-hexanol, zinc trifluoromethanesulfonate ($\text{Zn}(\text{OTf})_2$), and polytetrahydrofuran (PTHF, 2.9 kDa) were all purchased from Sigma-Aldrich. PTHF was dried at 80 °C under vacuum overnight before use. Dibutyltindilaurate (DBT, Alfa Aesar, MA, USA) and 4'-chloro-2, 2':6', 2''-terpyridine (chloride terpyridine, Fisher Scientific) were used as received.

Synthesis of 6-(2, 2':6', 2''-terpyridin-4'-yloxy)-hexan-1-amine (tpy-NH₂)

Powdered KOH (1.12 g, 20 mmol) was added to 30 mL dry dimethyl sulfoxide (DMSO) and the suspension was heated to 60 °C for 30 min. 6-Amino-1-hexanol (351.6 mg, 3.0 mmol) was then added and stirred at 60 °C for 1 h. Thereafter, chloride terpyridine (536 mg, 2.0 mmol) was added, and the resulting mixture was stirred at 60 °C for 36 h. After the reaction

mixture was cooled to room temperature, it was poured into deionized water (400 mL) to yield the precipitation of the product (tpy-NH₂), which was collected by filtration. The yellow solid was washed with deionized water (200 mL), and then dried in vacuum overnight at room temperature. The chemical structure of the tpy-NH₂ was confirmed by ¹H NMR spectra as shown in Figure S1.

Synthesis of terpyridine ligand-terminated CNT/PU prepolymer

The terpyridine-terminated polyurethane (PU) was prepared by *in situ* polymerization on the surface of multi-walled CNTs, as shown in Scheme 1. The hydroxyl-functionalized CNTs (14.0 mg, ~0.03 mmol OH, 1.0 eq) were dispersed in 20 mL anhydrous *N,N*-dimethylformamide (DMF) with the help of sonication for 30 min. HDI (48 μL, 0.3 mmol, 10 eq) and dibutyltin dilaurate (DBT, 6 μL) were then added to the mixture and stirred at 40 °C for 1 h. Dry PTHF (2.61 g, 0.9 mmol, 30 eq) and DBT (10 μL) dissolved in DMF (5 mL) were then added to the above mixture and further stirred at 40 °C for 2 h. Afterwards, HDI (192 μL, 1.2 mmol, 40 eq) was slowly injected into this reaction solution and stirred at 70 °C for 4 h to form a prepolymer containing CNTs. Tpy-NH₂ (209 mg, 0.6 mmol, 20 eq) was then added as the chain terminator and stirred at 70 °C for another 4 h to synthesize the terpyridine ligand-terminated CNT/PU prepolymer nanocomposite. The mixture was precipitated in cold menthol; the solid was collected by filtration and dried under vacuum overnight at room temperature.

Preparation of the metallo-supramolecular CNT/PU polymer nanocomposite films

Terpyridine ligand-terminated CNT/PU prepolymer (0.5 g) was dissolved in CHCl₃ (10 mL) in a 25 mL one neck flask with the help of sonication. Zn(OTf)₂ (1.0 mL, 0.05 mol L⁻¹) in acetonitrile was slowly added to the polymer solution under stirring. The mixture was then sonicated to remove air bubbles and transferred to a cylinder Teflon mold. The Teflon mold was placed at room temperature for 24 h to allow for slow drying. Traces of remaining solvent

were eliminated by vacuum drying for another 24 h. Dry films of about 0.13 mm in thickness were peeled off the Teflon mold for subsequent testing.

Characterization

The microstructure of the metallo-supramolecular CNT/PU polymer nanocomposite film was studied using a transmission electron microscope (TEM, Tecnai TF-30) with an accelerating voltage of 300 kV. For the TEM analysis, the sample (~70 nm in thickness) was prepared using a microtome (Reichert UltraCut E, NY USA). The self-healing characteristics of the films under different stimuli were monitored using a 3D optical interferometric profiler (Zygo NewView™ 7300). The thermal stability of the polymer film was characterized using a thermogravimetric analyzer (TGA, Q50 TA Instruments, USA) over a temperature range of 30 – 800 °C at a 10 °C min⁻¹ heating rate under an N₂ atmosphere. Differential scanning calorimetry (DSC) analyses were carried out in an N₂ atmosphere using a thermal analyzer (DSC, Q20 TA Instruments, USA) from –50 to 100 °C at a heating rate of 5 °C min⁻¹. Dynamic mechanical analyses were performed using a dynamic mechanical analyzer (DMA, TA Instruments RSA III, USA). X-ray diffraction (XRD) patterns were measured on a D8-Discovery diffractometer (Bruker, USA) with Cu K α radiation at a scanning rate of 5° min⁻¹. Small angle x-ray scattering (SAXS) measurements were carried out on a Rigaku SAX (Rigaku, USA). The wavelength of the X-ray was 0.154 nm and the sample-to-detector distance was 100 cm. The scattering vector is defined as $q = 4\pi \sin \theta / \lambda$, where 2θ is the scattering angle. Samples were mounted on a metal rack and fixed using tape. For temperature-dependent SAXS, the films were heated to a set temperature and stabilized thermally for 5 min. The FTIR spectra were studied using a Tensor 27 spectrometer (Bruker Daltonics Inc., USA) with 4 cm⁻¹ resolution at room temperature. ¹HNMR spectra were recorded on a Varian Mercury Plus 300 MHz spectrometer using DMSO as a solvent at 25 °C. Tensile tests were conducted using an Instron (Model 5967) fitted with a 250 N load cell. The

tensile strain rate was set at $50\% \text{ min}^{-1}$ for all tests. Virgin samples were cut into strips of $40 \text{ mm} \times 8 \text{ mm} \times 0.13 \text{ mm}$ using a razor and then measured. For the tensile test, at least five samples were measured, and the average results as well as the standard deviations were reported. The film temperature was measured using a K-type thermocouple. A silver wire detector was placed beneath the film to measure the temperature accurately.

Self-healing test

The healing efficiency was used to evaluate the healing performance of the metallo-supramolecular film, which was calculated based on the ratio between the toughness of the healed sample and that of the virgin sample. The toughness was calculated from the area under the tensile stress–strain curve. Metallo-supramolecular strips ($40 \text{ mm} \times 8 \text{ mm} \times 0.13 \text{ mm}$) were cut in the middle by a scalpel and all cuts were made perpendicular to the tensile direction (Figure S2). The sizes of the cuts were $\sim 4 \text{ mm}$ in length and $\sim 50 \mu\text{m}$ in depth. The cut samples were then healed by either near infrared (NIR) light, or heat, or solvent. For NIR light healing, an NIR laser with a wavelength of 803 nm was used as the light source. The NIR laser was positioned about 1.5 meters from the sample for 30 min , and the power density at the surface of the film was measured at $\sim 4.2 \text{ mW/mm}^2$ using a light intensity meter. For the NIR light-induced cyclic healing tests, the film was first cut and then exposed to NIR for 30 min . Thereafter, the film was allowed to cool down to room temperature for one hour. This process was referred to as the 1st healing cycle. After the 1st healing cycle, the same film was subjected to the same cutting, healing, and cooling process as described above and it was referred to as the 2nd healing cycle. The third healing cycle was conducted similarly on the same film after it was subjected to two healing cycles. For heat-induced healing, the cut film was heated at $90 \text{ }^\circ\text{C}$ on a hot plate for 1 h . For solvent-induced healing, two droplets of chloroform were dispensed to cover the cut once per hour for 3 h , and then the film was dried under vacuum for 24 h to eliminate the solvent. The cuts were monitored using a Zygo surface profilometer.

3. Results and Discussion

Materials Synthesis and Characterization

Commercially available hydroxyl-functionalized multi-walled CNTs were used for this study because (1) they can be uniformly dispersed in DMF solvent, and (2) the hydroxyl groups can readily react with the isocyanate groups. It has been previously demonstrated that a very low CNT loading level (e.g., 0.1–1.0 wt%) in the CNT/polymer nanocomposites can result in a rapid IR response.^{30, 31} For this study, the CNT loading content in the CNT/PU nanocomposites was 0.5 wt%. The CNTs were uniformly distributed in the PU matrix as shown in Figure S3. The synthesis of terpyridine ligand-terminated CNT/PU macromolecules is illustrated in Scheme 1. First, the hydroxyl-functionalized CNTs were reacted with a large excess of 1,6-hexyldiisocyanate (HDI) to ensure a complete reaction of the hydroxyl groups. The resulting mixture was then reacted with dihydroxyl poly(tetrahydrofuran) (PTHF, $M_n = 2900 \text{ g mol}^{-1}$), and subsequently reacted with the remaining excess HDI to form isocyanate functionalized prepolymers. Afterwards, 6-(2, 2':6', 2''-terpyridin-4'-yloxy)-hexan-1-amine (tpy-NH₂) was added as the chain terminator to produce the terpyridine ligand-terminated CNT/PU prepolymers. This dynamic self-healing system is based on the well-investigated terpyridine–metal ion complexation,³² where two terpyridine ligands coordinate with one Zn²⁺ ion to form a highly dynamic zinc–terpyridine complex. Therefore, the addition of Zn²⁺ into the terpyridine ligand-terminated CNT/PU prepolymer solution led to the formation of a gel via metal–ligand interaction (Scheme 2). The subsequent drying of the gel at room temperature resulted in the formation of a solid elastic film. For comparison, terpyridine-terminated CNT/PU nanocomposite film without the presence of Zn²⁺ (i.e., not crosslinked via the metal–ligand interaction) was also prepared and used as a control. In order to obtain a sufficient crosslinking density in the metallo-supromolecular polymer nanocomposite film, the feeding content of the terpyridine–NH₂ ligand was set at approximately 8%.^{23, 33} Complete

reaction of the terpyridine–NH₂ ligand was confirmed by FTIR (Figure S4) as the characteristic peak of NCO at 2260 cm⁻¹ was still present after reaction.

Figure 1 shows the typical tensile stress–strain curves of the CNT/PU nanocomposite films with or without (i.e., the control) Zn²⁺ coordination. The stress–strain curve of the Zn²⁺-coordinated film exhibited a sigmoid shape for the elastic polymer that was comprised of three regions:³⁴ (1) a linear elastic region at lower strain ($\epsilon < 50\%$) due to the straightening of the soft linker PTHF chain, (2) an intermediate region ($50\% < \epsilon < 250\%$) where the stress increased slowly with strain after reaching the yield point (i.e., $\sim 50\%$) due to plastic deformation, and (3) a strain-hardening region at higher strain ($\epsilon > 250\%$) where the polymer chains became highly orientated, thereby leading to strain-induced crystallization of the PTHF polymer segments.³⁵ The strain-induced PTHF crystallization was confirmed by X-ray diffraction (XRD) analysis as shown in Figure S5. Two distinct diffraction peaks located at $2\theta = 19.9^\circ$ and 24.3° were clearly observed for the stretched film and were attributed to the (002) and (202) lattice planes of the PTHF crystalline structure,³⁶ respectively. The control film showed an identical linear elastic region as the Zn²⁺-coordinated film at the low strain region, but the strain-hardening region was less obvious. The mechanical properties—including the Young's modulus, tensile strain-at-break, tensile strength, and the area under the stress–strain curve reflecting the toughness of the film—are summarized at Table 1. The presence of the metal–ligand interactions had a significant impact on the mechanical properties of the CNT/PU films, except for the Young's modulus. The tensile strength, tensile strain-at-break, and toughness of the films increased from 14.2 MPa, 620%, and 51.4 MPa to 22.8 MPa, 1076%, and 141.2 MPa, respectively, with the addition of Zn²⁺. The mechanical properties of the Zn²⁺-coordinated metallo-supramolecular film were also better than other self-healing materials reported in the literature,^{3, 15, 37, 38} which could potentially enhance their practical applications.

The thermal properties of polymeric materials are of great importance to their performance and application. The thermal stability of both the metallo-supramolecular film and the control film were measured by thermogravimetric analyzer (TGA) in a N_2 atmosphere, as shown in Figure 2a. It can be seen that both types of films were thermally stable up to 324.0 °C. The most significant weight loss occurred between 324.0 and 447.0 °C, and was attributed to the degradation of the PTHF chains.^{39, 40} In addition, both the Zn^{2+} -coordinated and control films were investigated using differential scanning calorimetry (DSC) analysis. The second heating and cooling runs of the DSC curves are shown in Figure 2b. No glass transition temperature (T_g) was observed during the heating cycle within the temperature range studied (i.e., -50 to 100 °C), suggesting that the T_g was likely out of the measurement range. Both the Zn^{2+} -coordinated and control films showed a strong PTHF melting peak at $T_m = 26.3$ °C. During the cooling cycle, the Zn^{2+} -coordinated and control films showed a strong PTHF crystallization peak at $T_c = -9.0$ °C and -15.1 °C, respectively, indicating that the metallo-supramolecular interaction likely promoted the crystallization of the PTHF polymer segment. In addition, both films retained their solid forms without any apparent change up to 100 °C at a macroscopic level.

Figure 2c and 2d show the dynamic temperature sweep results of the Zn^{2+} -coordinated film and control film at a frequency of 1 Hz and a strain of 0.1% with a heating rate of 5 °C min^{-1} . At 30 °C, the storage moduli (E') of both types of films were around 13 MPa. The storage modulus of the control film decreased much more dramatically with temperature than that of the Zn^{2+} -coordinated film within the temperature range studied (30 to 100 °C). For instance, the storage modulus of the Zn^{2+} -coordinated film and the control film at 80 °C was 10.0 and 4.9 MPa, respectively. Notably, the storage modulus of the Zn^{2+} coordinated metallo-supramolecular film exhibited a very mild change from 30 to 80 °C; whereas it showed a more apparent change above ~80 °C. This might be attributed to the decomplexation of the metal–ligand interactions above 80 °C.²⁴ The $\tan \delta$ value of the Zn^{2+} -coordinated

metallo-supramolecular film remained nearly constant within the temperature range studied (30 to 100 °C); while that of the control film increased with increasing temperature, indicating higher energy dissipation at higher temperatures.³⁴ These results demonstrated that the Zn²⁺-coordinated metallo-supramolecular film also possessed more desirable dynamic mechanical properties than the control film at high temperatures.

Self-Healing Properties

The self-healing capability is particularly desirable for multifunctional polymeric materials because it can make the materials more reliable, reduce repair costs, and extend the life of the material/product.^{3, 41, 42} The Zn²⁺-coordinated metallo-supramolecular nanocomposite film is unique in that it not only exhibited excellent mechanical properties and stretchability, but was also responsive to multiple stimuli, including remotely controlled NIR light, heat, and solvent. An optical profilometer was used to study the self-healing behaviors. For NIR light healing, a cut (Figure 3a; 48.3 μm in depth, ~50 μm in width, and ~4 mm in length) was generated using a scalpel on the metallo-supramolecular film. Thereafter, the cut was irradiated by NIR light (~4.2 mW/mm²) for 30 min and was allowed to cool. As shown in Figure 3b, the cut almost disappeared, with its depth decreasing from 48.3 to 3.1 μm, indicating an excellent healing ability by NIR light. The healed sample was able to sustain mechanical deformations including bending, stretching, and twisting without exacerbating the cut.

Essentially, the NIR-induced self-healing was due to the process of converting the light energy to thermal energy, which subsequently triggered the healing of the metallo-supramolecular film. Therefore, it is expected that the metallo-supramolecular nanocomposite film can be healed directly via thermal heat as well. As shown in Figure 4, after the cut (36.6 μm in depth, ~50 μm in width, and ~4 mm in length) on the metallo-supramolecular film was

heated at 90 °C for 1 h, the surface profilometry analysis revealed that the depth of the cut decreased from 36.6 to 2.1 μm .

Previous studies have found that the Zn^{2+} -terpyridine complex is highly dynamic in solution,³² thus the CNT/PU metallo-supramolecular film may also be healed by solvent. To test this hypothesis, a deep cut (55.5 μm in depth, \sim 50 μm in width, and \sim 4 mm in length) was created on the film by a scalpel (Figure 5a). Next, two droplets of chloroform were dispensed to cover the cut once per hour for 3 h, and then the film was dried under vacuum for 24 h to get rid of the solvent. As shown in Figure 5b, the cut disappeared after the cut was covered by chloroform for 3 h.

In order to quantitatively analyze the self-healing capabilities of the metallo-supramolecular film, tensile tests were carried out for the virgin films (i.e., without any cut), films with a fresh cut, NIR-healed film, heat-healed film, and solvent-healed film (Figure 6a). It is apparent that the 0.5 wt% CNT/PU metallo-supramolecular film was healed very well by all three types of stimuli including NIR light, heat, and solvent. As shown in Table 2 and Figure 6, the toughness ratio between the cut sample and the virgin sample ($Toughness_{\text{cut}}/Toughness_{\text{virgin}}$) was 28% before any treatment with NIR, heat, or solvent, while the toughness ratio between the healed sample and the virgin sample ($Toughness_{\text{healed}}/Toughness_{\text{virgin}}$) was approximately 97, 95, and 93%, respectively, for the NIR-, heat-, and solvent-healed films, respectively, suggesting a very high healing efficiency for all three types of stimuli. In other words, the mechanical properties of the films were almost completely restored upon NIR, heat, or solvent treatment, which is remarkable. More importantly, the metallo-supramolecular film still maintained 84% and 80% of its initial toughness after the 2nd and 3rd cyclic NIR light-induced healing test (Figure S7), respectively, indicating that the metallo-supramolecular film was capable of repeated healing cycles.

Many polymers show certain degrees of thermo/chemo-responsive shape memory effects albeit with different recovery capabilities.⁴³ Interestingly, the metallo-supramolecular

film was capable of complete shape recovery after thermal treatment indicating an excellent thermally induced shape memory effect. As shown in Figure S8a, a metallo-supramolecular film strip was initially stretched from 3.4 to 25 cm, and its length was recovered to ~12.5 cm after the force was removed. However, the stretched film strip was fully recovered to its original length after it was heated at 80 °C for 2 min (cf. Movie S1 in the Supporting Information). For comparison purposes, a control film was stretched from 3.4 to 17 cm, and retracted to ~10 cm after releasing the force. Its length only retracted to 5.5 cm after being heated at 80 °C for 2 min (Figure S8b and Movie S1 in the Supporting Information). The excellent shape memory effect exhibited by the metallo-supramolecular film may be attributed to these factors: (1) melting of the strain-induced crystalline polymer regions during the thermal treatment, and (2) the dynamic metal–ligand bonds serving as a reversible phase for the shape memory.^{38,44}

Li et al. proposed a biomimic two-step self-healing mechanism with the first step being crack sealing via the shape memory effect and the second step being healing via different approaches.^{45,46} This two-step self-healing mechanism may also be applicable to our self-healing materials. According to the DSC curve shown in Figure 2b, the glass transition temperature (T_g) of the metallo-supramolecular film was below -50°C and the melting temperature of the localized PTHF crystalline regions was 26 °C. Although the metallo-supramolecular film retained its solid form up to 100 °C at a macroscopic level, the crack surfaces in the heated (either via NIR irradiation or direct heating) polymer film started to seal due to the shape memory effect as described above. As discussed in the paragraph below, the second step, i.e., the healing step, was attributed to the decomplexation of the metal-ligand bonds and dissociation of ionic clusters occurred at elevated temperature,^{23, 24, 47} and the subsequent re-complexation of the metal-ligand bonds and reorganization of ionic clusters upon cooling, that led to complete healing of the cut film and the recovery of its mechanical properties.

The superior healing performance of the 0.5 wt% CNT/PU metallo-supramolecular film by NIR light can be ascribed to several factors. (1) CNTs have excellent NIR light absorption and thermal conversion capabilities.^{25, 30} Therefore, the numerous well-dispersed CNTs present in the metallo-supramolecular film can absorb the NIR light efficiently and convert it to thermal energy.³⁰ In addition, CNTs can efficiently transfer thermal energy within the polymer matrix due to their excellent thermal conductivity.⁴⁸ Therefore, upon exposure to NIR light, the metallo-supramolecular film heated rapidly and uniformly, as demonstrated by the temperature profile in the supporting information (Figure S9). The temperature of the metallo-supramolecular polymer nanocomposite film increased rapidly upon NIR irradiation (4.2 mW mm⁻²) and reached a plateau (~100 °C) after ~2 minutes. (2) Due to the highly dynamic nature of the Zn²⁺-terpyridine interaction, the thermal energy generated by the IR absorption of CNTs could trigger the decomplexation of the Zn²⁺-terpyridine bonds leading to the subsequent reformation of the Zn²⁺-terpyridine bonds (upon cooling) at the cut/crack surface and thus healing of the film. The self-healing mechanism based on decomplexation/complexation of the dynamic metal-ligand interaction has been previously reported by Rowan and colleagues.²⁴ (3) Ionic clusters were formed by several complexes interacting with negatively charged counter ions (i.e., trifluoromethanesulfonate).^{23, 33} This was supported by the small angle X-ray scattering (SAXS) measurements (Figure S10). The Zn²⁺-coordinated metallo-supramolecular film revealed a broad scattering peak at $q = 0.45 \text{ nm}^{-1}$, corresponding to a distance ($d = 2\pi/q$) of 13.9 nm. Partial dissociation of an ionic cluster (Figure S11) at high temperatures (>80 °C) followed by reorganization (upon cooling) could also possibly contribute to the self-healing behavior of the film.⁴⁷ The superior NIR-induced self-healing ability allows for remotely controlled and localized repairs, thereby enabling *in situ* repairs and thus minimizing potential damage to the surrounding materials/structures, which would greatly expand their application. Similarly, the superior heat-induced healing performance can be attributed to the decomplexation and subsequent re-

complexation of the Zn^{2+} -terpyridine complexes at higher temperatures ($>80\text{ }^{\circ}\text{C}$), as well as the rearrangement/reorganization of the ionic clusters.^{23, 24, 47}

The excellent solvent healing capability was attributed to the dynamic nature of the Zn^{2+} -terpyridine interaction. Upon a fresh cut, some polymer chains and metal–ligand complexes were damaged.^{21, 34} The presence of a solvent allowed for the polymer chains, uncomplexed zinc ions, and terpyridine ligands, as well as certain metal–ligand complexes, to diffuse towards the cut surfaces. The subsequent ligand exchanges and formation of new complexes led to the healing of the cut.

In order to further confirm the essential role of the dynamic metal–ligand interactions for the self-healing behavior of the 0.5 wt% CNT/PU metallo-supramolecular nanocomposite films, the control films (i.e., without the presence of Zn^{2+}) were subjected to the same self-healing tests (i.e., generating a fresh cut followed by treatment with NIR light, heat, or solvent). Tensile tests were carried out to investigate the healing performances of the control films. As shown in Figure S12 and Table S1, the healing performances were generally very poor. More specifically, while the toughness ratio ($Toughness_{\text{cut}}/Toughness_{\text{virgin}}$) between the cut sample and the virgin sample was 33% before any treatments (e.g., solvent, NIR, or heat), the toughness ratio between the solvent-treated control film and the original control film was only about 34%, suggesting that the solvent was ineffective in healing the control film. The toughness ratio between the NIR light-treated control sample and the original control sample was approximately 45%. Similarly, the toughness ratio between the heat-treated control sample and the original control sample was also about 45%. Thus, the healing efficiency induced by both NIR and heat were very low in the control film. The minor healing effects induced by NIR and heat may be attributed to polymer chain diffusion and re-entanglement at higher temperatures.³⁸ Collectively, these experiments confirmed that the presence of dynamic supramolecular metal–ligand interaction was of great importance for effective healing.

4. Conclusions

A novel self-healing metallo-supramolecular polymer nanocomposite was prepared by *in situ* polymerization of polyurethane followed by crosslinking with Zn^{2+} ion. The resulting Zn^{2+} -coordinated metallo-supramolecular CNT/PU polymer nanocomposite possessed remarkable mechanical properties owing to the metallo-supramolecular interactions. Furthermore, the dynamic nature of the metal–ligand interactions endowed the CNT/PU nanocomposite with rapid and efficient self-healing capabilities under three different stimuli, including remotely controlled NIR light, heat, and a solvent. Thus, the combination of superior mechanical properties and outstanding self-healing capabilities may offer the metallo-supramolecular polymer nanocomposite many promising applications including as structural components, microelectronics, sporting equipment, and artificial skins. Finally, the metallo-supramolecular polymer nanocomposite film also exhibited a thermally induced shape memory effect that can lead to other applications.

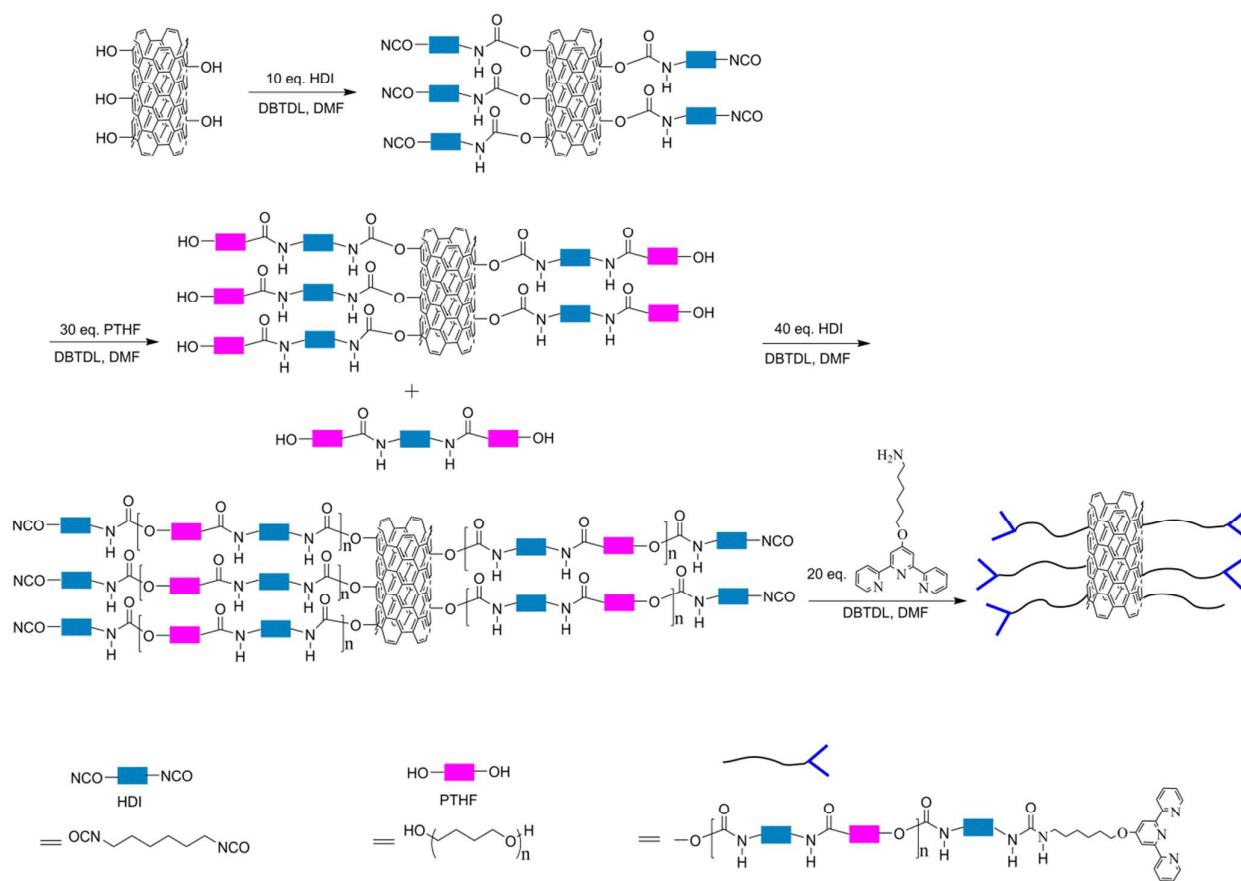
Acknowledgements

The authors gratefully acknowledge the financial support from the University of Wisconsin–Madison.

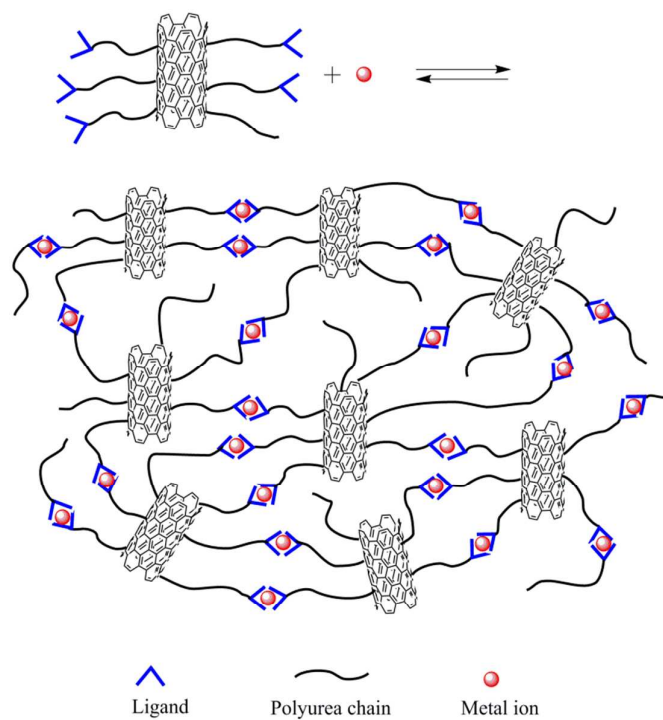
References

1. F. Hussain, M. Hojjati, M. Okamoto and R. E. Gorga, *Journal of Composite Materials*, 2006, **40**, 1511-1575.
2. L. M. Robeson, *Polymer Engineering & Science*, 1984, **24**, 587-597.
3. Y. Yang and M. W. Urban, *Chem Soc Rev*, 2013, **42**, 7446-7467.
4. D. Y. Wu, S. Meure and D. Solomon, *Progress in Polymer Science*, 2008, **33**, 479-522.
5. K. Kratz, A. Narasimhan, R. Tangirala, S. Moon, R. Revanur, S. Kundu, H. S. Kim, A. J. Crosby, T. P. Russell, T. Emrick, G. Kolmakov and A. C. Balazs, *Nat Nano*, 2012, **7**, 87-90.
6. S. R. White, N. R. Sottos, P. H. Geubelle, J. S. Moore, M. R. Kessler, S. R. Sriram, E. N. Brown and S. Viswanathan, *Nature*, 2001, **409**, 794-797.
7. M. M. Caruso, B. J. Blaiszik, H. Jin, S. R. Schelkopf, D. S. Stradley, N. R. Sottos, S. R. White and J. S. Moore, *Acs Appl Mater Inter*, 2010, **2**, 1195-1199.
8. H. R. Williams, R. S. Trask, P. M. Weaver and I. P. Bond, *Journal of The Royal Society Interface*, 2008, **5**, 55-65.
9. K. S. Toohy, N. R. Sottos, J. A. Lewis, J. S. Moore and S. R. White, *Nat Mater*, 2007, **6**, 581-585.
10. B. J. Adzima, C. J. Kloxin and C. N. Bowman, *Adv Mater*, 2010, **22**, 2784-2787.
11. X. Chen, M. A. Dam, K. Ono, A. Mal, H. Shen, S. R. Nutt, K. Sheran and F. Wudl, *Science*, 2002, **295**, 1698-1702.
12. C.-M. Chung, Y.-S. Roh, S.-Y. Cho and J.-G. Kim, *Chemistry of Materials*, 2004, **16**, 3982-3984.
13. J. Canadell, H. Goossens and B. Klumperman, *Macromolecules*, 2011, **44**, 2536-2541.
14. Y. Chen, A. M. Kushner, G. A. Williams and Z. Guan, *Nat Chem*, 2012, **4**, 467-472.
15. P. Cordier, F. Tournilhac, C. Soulie-Ziakovic and L. Leibler, *Nature*, 2008, **451**, 977-980.
16. M. Zhang, D. Xu, X. Yan, J. Chen, S. Dong, B. Zheng and F. Huang, *Angewandte Chemie International Edition*, 2012, **51**, 7011-7015.
17. S. Burattini, B. W. Greenland, D. H. Merino, W. Weng, J. Seppala, H. M. Colquhoun, W. Hayes, M. E. Mackay, I. W. Hamley and S. J. Rowan, *J Am Chem Soc*, 2010, **132**, 12051-12058.
18. X. Wang, F. Liu, X. Zheng and J. Sun, *Angewandte Chemie International Edition*, 2011, **50**, 11378-11381.
19. N. Holtén-Andersen, M. J. Harrington, H. Birkedal, B. P. Lee, P. B. Messersmith, K. Y. C. Lee and J. H. Waite, *Proceedings of the National Academy of Sciences*, 2011, **108**, 2651-2655.
20. M. J. Harrington, A. Masic, N. Holtén-Andersen, J. H. Waite and P. Fratzl, *Science*, 2010, **328**, 216-220.
21. J. Yuan, X. Fang, L. Zhang, G. Hong, Y. Lin, Q. Zheng, Y. Xu, Y. Ruan, W. Weng, H. Xia and G. Chen, *Journal of Materials Chemistry*, 2012, **22**, 11515-11522.
22. H.-P. Cong, P. Wang and S.-H. Yu, *Chemistry of Materials*, 2013, **25**, 3357-3362.
23. S. Bode, L. Zedler, F. H. Schacher, B. Dietzek, M. Schmitt, J. Popp, M. D. Hager and U. S. Schubert, *Adv Mater*, 2013, **25**, 1634-1638.
24. M. Burnworth, L. Tang, J. R. Kumpfer, A. J. Duncan, F. L. Beyer, G. L. Fiore, S. J. Rowan and C. Weder, *Nature*, 2011, **472**, 334-337.
25. P. M. Ajayan, *Chem Rev*, 1999, **99**, 1787-1800.
26. Q. Zheng, A. Javadi, R. Sabo, Z. Cai and S. Gong, *RSC Advances*, 2013, **3**, 20816-20823.
27. P. W. Barone, S. Baik, D. A. Heller and M. S. Strano, *Nat Mater*, 2005, **4**, 86-92.

28. T. W. Ebbesen, H. J. Lezec, H. Hiura, J. W. Bennett, H. F. Ghaemi and T. Thio, *Nature*, 1996, **382**, 54-56.
29. X. Wan, J. Dong and D. Y. Xing, *Phys Rev B*, 1998, **58**, 6756-6759.
30. R. R. Kohlmeier, M. Lor and J. Chen, *Nano Letters*, 2012, **12**, 2757-2762.
31. L. Yang, K. Setyowati, A. Li, S. Gong and J. Chen, *Adv Mater*, 2008, **20**, 2271-2275.
32. A. Wild, A. Winter, F. Schlutter and U. S. Schubert, *Chem Soc Rev*, 2011, **40**, 1459-1511.
33. S. Bode, R. K. Bose, S. Matthes, M. Ehrhardt, A. Seifert, F. H. Schacher, R. M. Paulus, S. Stumpf, B. Sandmann, J. Vitz, A. Winter, S. Hoepfener, S. J. Garcia, S. Spange, S. van der Zwaag, M. D. Hager and U. S. Schubert, *Polym Chem-Uk*, 2013, **4**, 4966-4973.
34. G. Hong, H. Zhang, Y. Lin, Y. Chen, Y. Xu, W. Weng and H. Xia, *Macromolecules*, 2013, **46**, 8649-8656.
35. B. X. Fu, B. S. Hsiao, S. Pagola, P. Stephens, H. White, M. Rafailovich, J. Sokolov, P. T. Mather, H. G. Jeon, S. Phillips, J. Lichtenhan and J. Schwab, *Polymer*, 2001, **42**, 599-611.
36. R. Rachmawati, A. J. J. Woortman and K. Loos, *Macromolecular Bioscience*, 2013, **13**, 767-776.
37. J. Li, G. Zhang, L. Deng, S. Zhao, Y. Gao, K. Jiang, R. Sun and C. Wong, *Journal of Materials Chemistry A*, 2014, **2**, 20642-20649.
38. Z. Wang, W. Fan, R. Tong, X. Lu and H. Xia, *RSC Advances*, 2014, **4**, 25486-25493.
39. Y. Hattab and N. Benharrats, *Arabian Journal of Chemistry*, 2015, **8**, 285-292.
40. T. C. Chang, K. H. Wu, H. B. Chen, S. Y. Ho and Y. S. Chiu, *Journal of Polymer Science Part A: Polymer Chemistry*, 1996, **34**, 3337-3343.
41. X. Xiao, T. Xie and Y.-T. Cheng, *Journal of Materials Chemistry*, 2010, **20**, 3508-3514.
42. S. D. Bergman and F. Wudl, *Journal of Materials Chemistry*, 2008, **18**, 41-62.
43. W. M. Huang, Y. Zhao, C. C. Wang, Z. Ding, H. Purnawali, C. Tang and J. L. Zhang, *Journal of Polymer Research*, 2012, **19**, 1-34.
44. J. R. Kumpfer and S. J. Rowan, *J Am Chem Soc*, 2011, **133**, 12866-12874.
45. G. Li and N. Uppu, *Composites Science and Technology*, 2010, **70**, 1419-1427.
46. J. Nji and G. Li, *Polymer*, 2010, **51**, 6021-6029.
47. S. Kupfer, L. Zedler, J. Guthmuller, S. Bode, M. D. Hager, U. S. Schubert, J. Popp, S. Grafe and B. Dietzek, *Phys Chem Chem Phys*, 2014, **16**, 12422-12432.
48. L. Huang, N. Yi, Y. Wu, Y. Zhang, Q. Zhang, Y. Huang, Y. Ma and Y. Chen, *Adv Mater*, 2013, **25**, 2224-2228.



Scheme 1. Synthesis of the terpyridine ligand-terminated CNT/PU prepolymer nanocomposite.



Scheme 2. The terpyridine ligand-terminated CNT/PU prepolymer nanocomposite crosslinked with Zn^{2+} ions forming the metallo-supramolecular CNT/PU polymer nanocomposite.

Table 1. The mechanical properties of the CNT/PU nanocomposite films with or without (i.e., the control) Zn^{2+} coordination.

Sample	Young's modulus (MPa)	Tensile strain- at-break (%)	Tensile strength (MPa)	Toughness (MPa)
Zn^{2+}	6.3 ± 0.2	1076 ± 30	22.8 ± 0.3	141.2 ± 1.5
Control	6.2 ± 0.3	658 ± 22	14.2 ± 0.3	51.4 ± 1.2

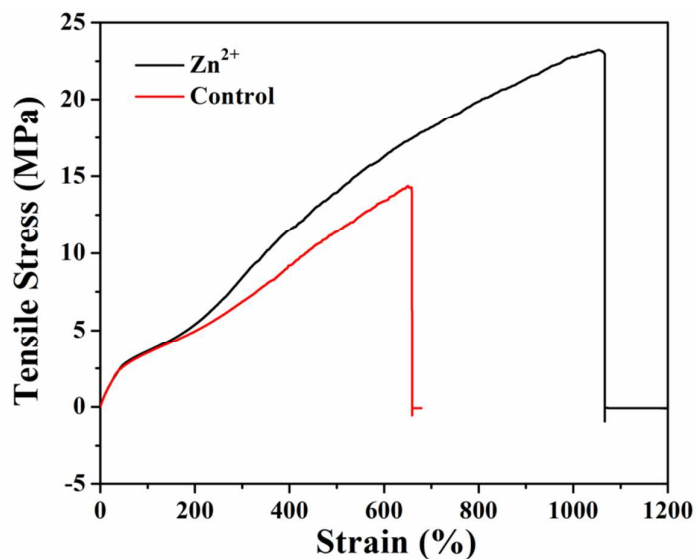


Figure 1. Tensile stress vs. strain curve of the CNT/PU nanocomposite films with or without (i.e., the control) Zn²⁺ coordination.

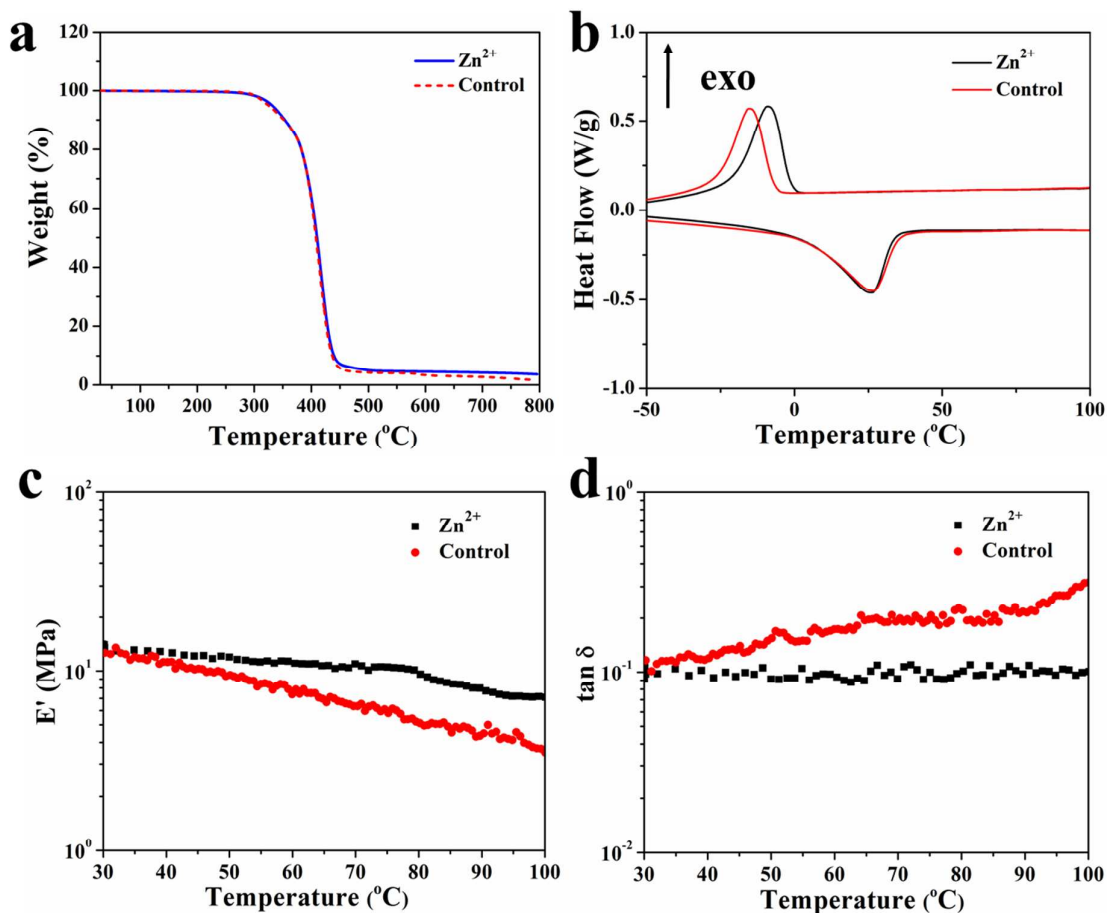


Figure 2. (a) TGA curves and (b) DSC curves of the Zn^{2+} -coordinated supramolecular film and control film. (c) The storage moduli, and (d) the tangent of the phase angle ($\tan \delta$) of the Zn^{2+} -coordinated supramolecular film and control film.

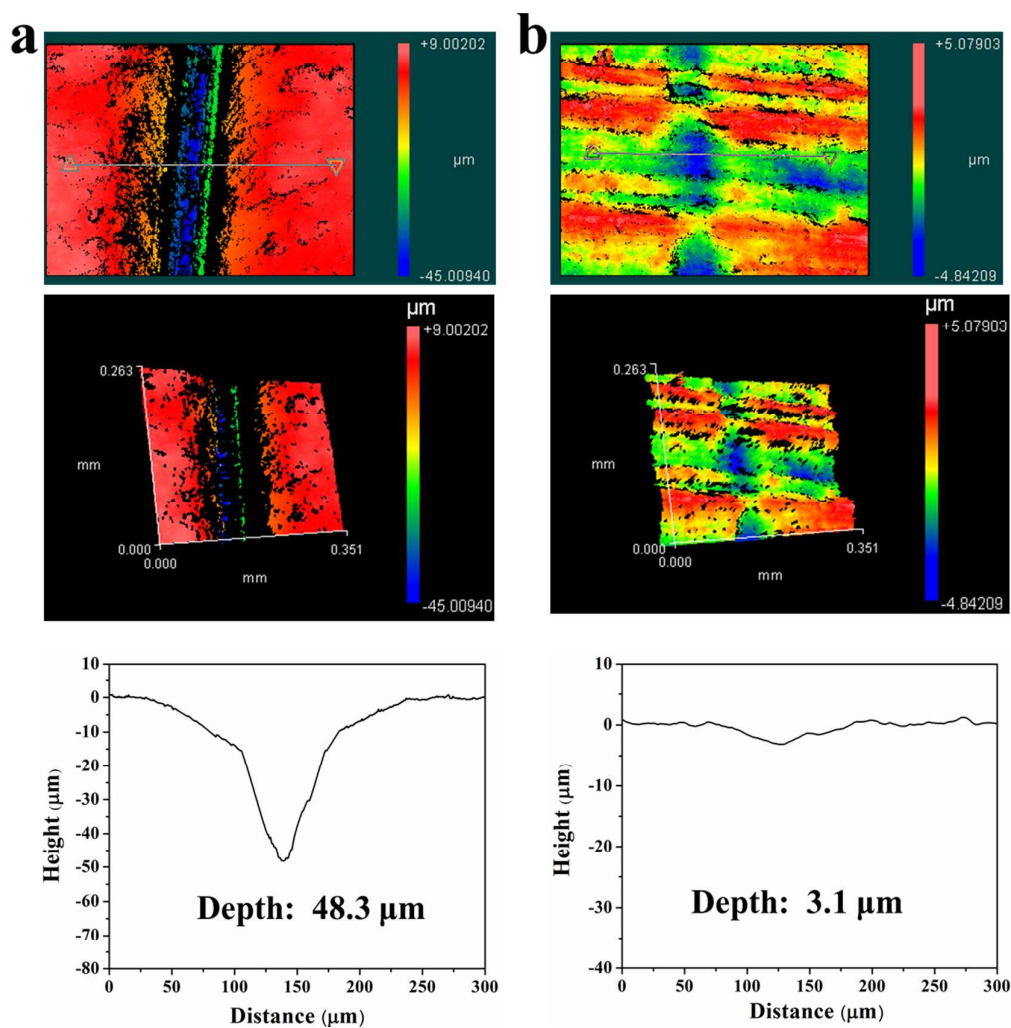


Figure 3. Surface profilometry measurement of the Zn^{2+} -coordinated supramolecular film after being (a) cut with a scalpel, and (b) healed with NIR light.

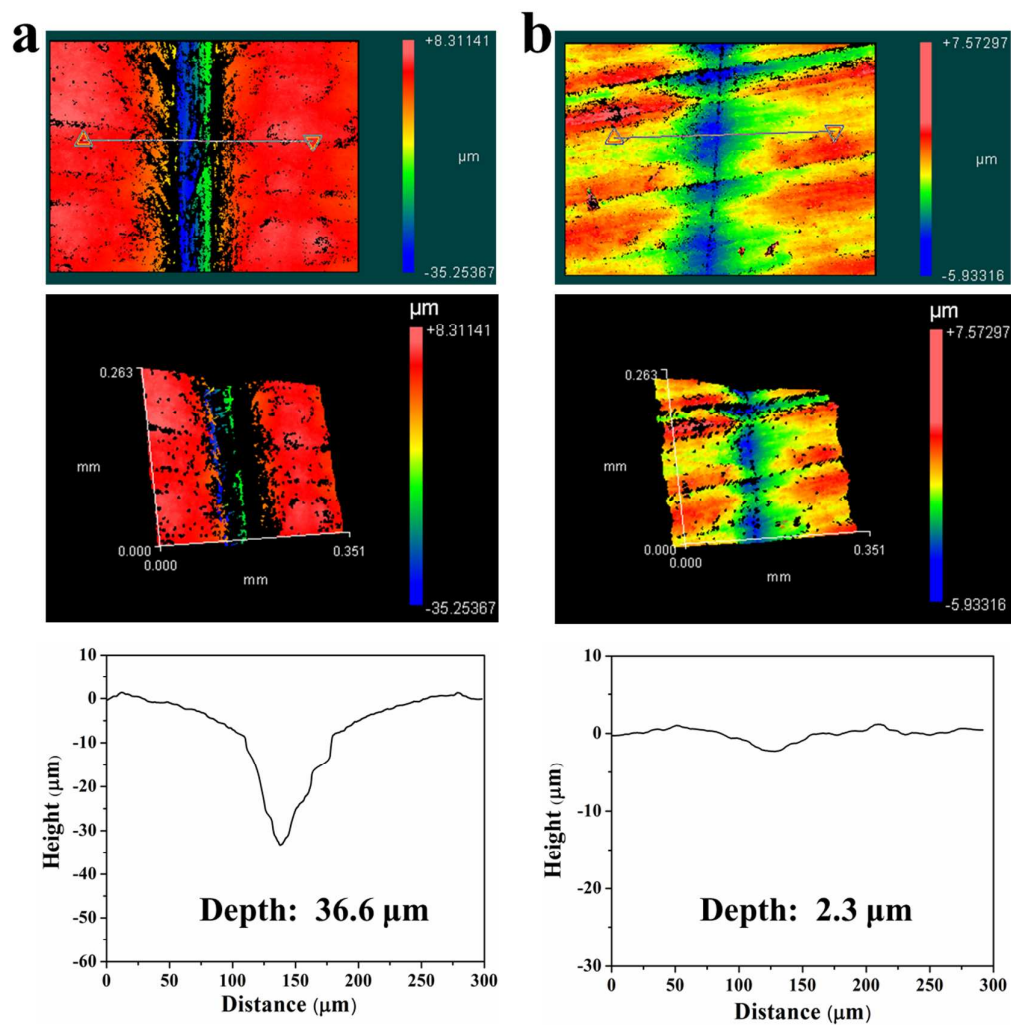


Figure 4. The surface profilometry measurement of the Zn²⁺-coordinated supramolecular film after being (a) cut with a scalpel, and (b) healed with heat.

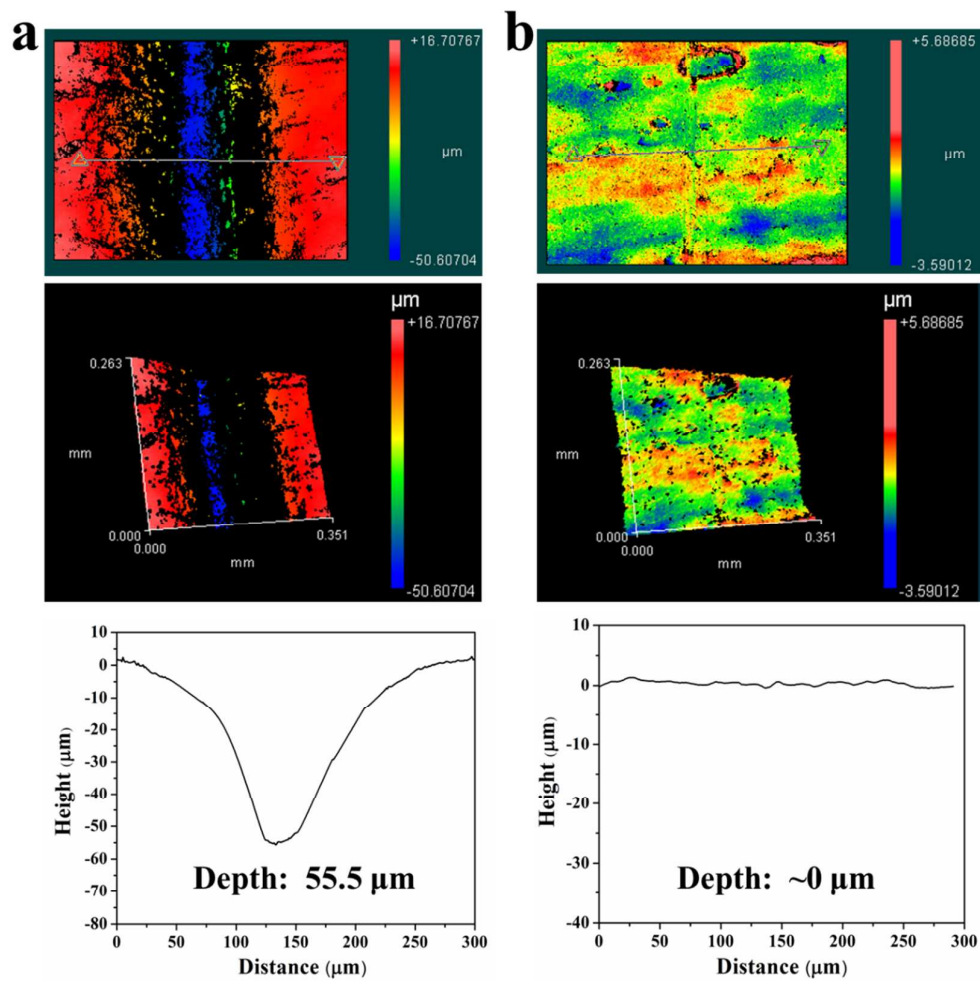


Figure 5. The surface profilometry measurement of the Zn²⁺-coordinated supramolecular film after being (a) cut with a scalpel, and (b) healed with solvent.

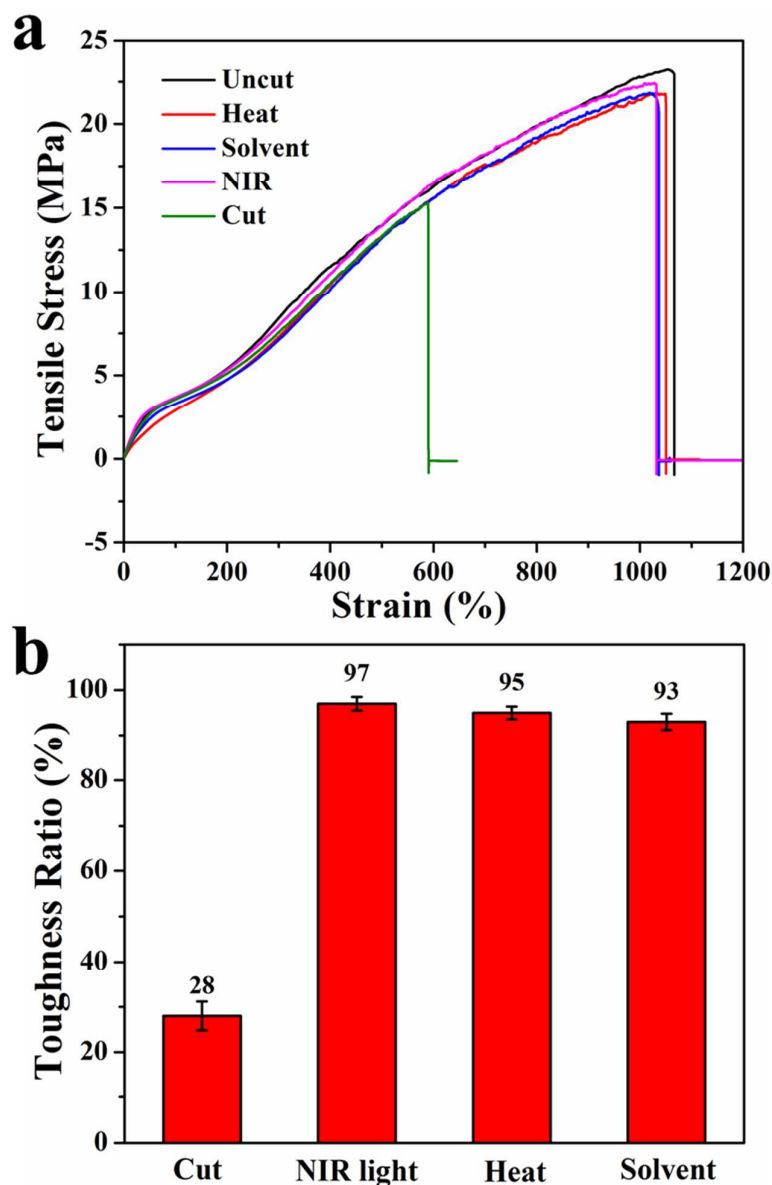


Figure 6. (a) The tensile stress–strain curves of the 0.5 wt% CNT/PU supramolecular film including the uncut film, NIR light-healed film, heat-healed film, solvent-healed film, and freshly cut film. (b) The toughness ratio of the 0.5 wt% CNT/PU supramolecular film including the cut film before any treatment, and the cut film healed via NIR, heat, and solvent. The healing efficiency was calculated based on the ratio of the calculated toughness (i.e., the area under the stress–strain curve) of the healed and virgin films.

Table 2. The mechanical properties of the metallo-supramolecular films including the uncut film, freshly cut film, NIR light-treated film, heat-treated film, and solvent-treated film.

Sample	Young's modulus (MPa)	Tensile strain- at-break (%)	Tensile strength (MPa)	Toughness (MPa)
Uncut	6.3 ± 0.2	1076 ± 30	22.8 ± 0.3	141.2 ± 1.5
NIR light	6.4 ± 0.2	1028 ± 25	22.4 ± 0.2	137.3 ± 1.4
Heat	4.6 ± 0.3	1048 ± 28	21.8 ± 0.3	134.0 ± 2.0
Solvent	6.2 ± 0.3	1018 ± 42	21.8 ± 0.4	131.7 ± 2.3
Cut	6.1 ± 0.7	574 ± 95	15.0 ± 2.6	40.2 ± 8.4